

Published in final edited form as:
*Geophys Res Lett*. 2018 October 16; 45(19): 10,456–10,463. doi:10.1029/2018GL079031.

# Global retrievals of solar induced chlorophyll fluorescence with TROPOMI: first results and inter-sensor comparison to OCO-2

**Philipp Köehler**[1], **Christian Frankenberg**[1,2], **Troy S. Magney**[2], **Luis Guanter**[3], **Joanna Joiner**[4], **Jochen Landgraf**[5]

[1]Division of Geological and Planetary Sciences, California Institute of Technology, Pasadena, CA, USA [2]Jet Propulsion Laboratory, California Institute of Technology, Pasadena, CA, USA [3]Helmholtz Centre Potsdam, German Research Center for Geosciences (GFZ), Potsdam, Germany [4]NASA Goddard Space Flight Center, Greenbelt, MD, USA [5]SRON Netherlands Institute for Space Research, Utrecht, Netherlands

## Abstract

In recent years, solar-induced chlorophyll fluorescence (SIF) retrieved from space borne spectrometers has been extensively used as a proxy for terrestrial photosynthesis at relatively sparse temporal and spatial scales. The near-infrared band of the recently launched TROPOspheric Monitoring Instrument (TROPOMI) features the required spectral resolution and signal-to-noise ratio to retrieve SIF in a spectral range devoid of atmospheric absorption features. We find that initial TROPOMI spectra meet high expectations for a substantially improved spatio-temporal resolution (up to 7 km × 3.5 km pixels with daily revisit), representing a step change in SIF remote sensing capabilities. However, interpretation requires caution, as the broad range of viewing-illumination geometries covered by TROPOMI's 2600 km wide swath needs to be taken into account. A first inter-sensor comparison with OCO-2 (Orbiting Carbon Observatory-2) SIF shows excellent agreement, underscoring the high quality of TROPOMI's SIF retrievals and the notable radiometric performance of the instrument.

**Plain Language Summary—**Photosynthesis is the most essential process for life on Earth, but gradually changing environmental conditions such as increasing concentrations of atmospheric trace gases, rising temperatures or reduced water availability could adversely affect the photosynthetic productivity. The recently launched TROPOspheric Monitoring Instrument (TROPOMI) is designed to monitor atmospheric trace gases and air pollutants with an unprecedented resolution in space and time, while its radiometric performance also permits us to see a weak electromagnetic signal emitted by photosynthetically active vegetation - solar induced chlorophyll fluorescence (SIF). Mounting evidence suggests that SIF observations from satellite instruments augment our abilities to track the photosynthetic performance and carbon uptake of terrestrial vegetation. In this study, we present the first TROPOMI SIF retrievals, largely

Philipp Köehler and Christian Frankenberg, pkoehler@caltech.edu, cfranken@caltech.edu.

outperforming previous and existing capabilities for a spatial continuous monitoring of SIF from space.

## 1. Introduction

Accurate knowledge of gross primary production (GPP) through photosynthesis is crucial for understanding the land-atmosphere carbon exchange with associated climate feedbacks. Solar induced chlorophyll fluorescence (SIF) is regarded as a powerful proxy for photosynthesis as it is linked to the electron transport in the light reactions of photosynthesis. SIF is a weak electromagnetic signal (spectrally smooth double peak feature with maximum values in the red and far red) emitted from excited chlorophyll *a* molecules after absorption of photosynthetically active radiation (PAR). Multiple global SIF data sets have recently become available from satellite instruments initially designed for atmospheric remote sensing [e.g., *Frankenberg et al.*, 2011a; *Joiner et al.*, 2011, 2012, 2013; *Guanter et al.*, 2012; *Köhler et al.*, 2015a, b; *Wolanin et al.*, 2015]. Even though none of these observations provided the spatio-temporal resolution and coverage typically required for surface vegetation remote sensing, a strong empirical linear relationship between SIF and estimates of GPP was discovered [*Frankenberg et al.*, 2011b; *Guanter et al.*, 2012]. Despite an incomplete mechanistic understanding [e.g., *Porcar-Castell et al.*, 2014], there is mounting evidence that global SIF data sets can track GPP dynamics in several ecosystems, such as tropical rainforests [*Lee et al.*, 2013; *Parazoo et al.*, 2013; *Guan et al.*, 2015], crop- and grasslands [*Guanter et al.*, 2014; *Zhang et al.*, 2014; *Wood et al.*, 2017; *Jeong et al.*, 2017; *Verma et al.*, 2017], boreal forests [*Walther et al.*, 2016; *Zhang et al.*, 2016], and temperate deciduous forest [*Yang et al.*, 2015]. Notably, SIF may provide an ideal GPP constraint for Terrestrial Biosphere Models [e.g., *Parazoo et al.*, 2014; *Thum et al.*, 2017; *MacBean et al.*, 2018]. Improvements in spatial resolution and coverage of SIF observations will enable a more mechanistic understanding of the SIF signal. In this regard, the TROPOspheric Monitoring Instrument (TROPOMI) promises a step-change.

So far, gridded SIF data sets have a limited temporal and spatial resolution (0.5° – 2°), which can either be attributed to a large footprint size in case of GOME-2 (Global Ozone Monitoring Experiment-2) and SCIAMACHY (SCanning Imaging Absorption SpectroMeter for Atmospheric CHartographY) or to sparse and spatially discontinuous measurements from GOSAT (Greenhouse Gases Observing Satellite) and OCO-2 (Orbiting Carbon Observatory-2). TROPOMI builds upon the heritage of space borne spectrometers such as SCIAMACHY and GOME-2, but enables a substantial improvement in SIF monitoring due to a small footprint size (7 km × 3.5 km at nadir) compared to GOME-2 (40 km × 40 km) and SCIAMACHY (30 km × 60 km), while providing almost daily spatially continuous global coverage as opposed to GOSAT and OCO-2. TROPOMI SIF can potentially reveal detailed patterns in space and time, improving our ability to examine the relationship between photosynthesis and SIF at ecologically meaningful scales. In addition, SIF retrievals can also detect unexpected instrumental issues affecting other retrievals, as it is very sensitive to additive offsets in the measured radiances. For example, *Frankenberg et al.* [2011b] found a radiance level dependent offset in the O2-A band of GOSAT-FTS spectra, caused by a zero-level offset in the FTS interferogram. For OCO-2, the SIF retrieval also uncovered a small time-dependent offset due to the formation of a very thin ice layer on the

focal plane array [*Crisp et al.*, 2017; *Sun et al.*, 2017]. As such, SIF studies in the initial phase of a satellite mission can provide useful insights into potential calibration issues.

In this study, we briefly describe the instrument and highlight TROPOMI-specific measurement features, which are essential for interpretation. We further outline our SIF retrieval approach, present the first global TROPOMI SIF observations, and conduct an inter-sensor comparison with co-located OCO-2-SIF observations.

## 2. Data and Retrieval

### 2.1. TROPOMI - Instrument Overview

TROPOMI [ *Veefkind et al.*, 2012] is the single payload of the Sentinel 5 Precursor (S-5P) satellite, which was successfully launched on 13 October 2017. S-5P flies in a near-polar, sun-synchronous orbit in an altitude of 824 km with an equatorial crossing at 13:30 h Local Solar Time (LST) and a repeat cycle of 17 days. The instrument's wide swath width of approximately 2600 km enables almost daily global surface coverage (100% for latitudes greater than +/−7°, better than 95% coverage in between). Integrating the reflected sunlight every second with a two-dimensional (across swath, wavelength) detector results in a spatial resolution of 7 km along track and 3.5–15 km across track, depending on the view angle and detector pixel co-adding (see Sect. S1 for details). TROPOMI is designed to monitor atmospheric trace gases (including CO, $CH_4$, $O_3$, $NO_2$, $SO_2$) as well as cloud and aerosol properties. These data are crucial for monitoring the atmospheric composition and to detect air pollutants with an unprecedented accuracy and spatio-temporal resolution [*Hu et al.*; *Borsdorff et al.*, 2018]. Coincidentally, TROPOMI's near-infrared (NIR) band 6 (725 nm-775 nm, FWHM=0.38 nm) covers the far-red part of the SIF emission spectrum, allowing for its retrieval. Previous studies [e.g., *Joiner et al.*, 2013; *Wolanin et al.*, 2015; *Köhler et al.*, 2015b] already demonstrated the feasibility of retrieving SIF from space borne atmospheric spectrometers with similar spectral characteristics (SCIAMACHY, FWHM=0.48 nm; GOME-2, FWHM=0.5 nm). Building on the aforementioned studies, *Guanter et al.* [2015] outlined the potential of TROPOMI with regard to the retrieval of SIF as well as other vegetation parameters.

### 2.2. Important Measurement Features

Owing to its wide swath, several issues for the interpretation of TROPOMI SIF arise, specifically related to the sun-surface-sensor geometry. Fig. 1 (a) demonstrates that a considerable LST span (11:30 LST – 18:15 LST) is covered within the sunlit portion of its orbit (solar zenith angles < 70°). The LST of an arbitrary measurement should not be confused with the nominal satellite overpass time (13:30 LST), which is only equivalent for nadir soundings when the satellite passes the equator (up to ±1 h for non-nadir soundings). This differentiation is important, because SIF is driven by instantaneous PAR, which changes over the course of a day. *Frankenberg et al.* [2011b] proposed a simple approach to convert instantaneous SIF to a daily average, which accounts for variations in overpass time, length of day, and solar zenith angle

$$\overline{SIF} = SIF(t_m) \cdot \frac{1}{\cos(\theta(t_m))} \int_{t=t_m-12h}^{t=t_m+12h} \cos(\theta(t)) \cdot H(\cos(\theta(t)))dt, \quad (1)$$

where $\theta(t_m)$ is the solar zenith angle at the time of measurement $t_m$, and the integral is computed numerically in 10 minute time-steps ($dt$), with the heaviside step function $H$ zeroing out negative values of $\cos(\theta)$. The overall scaling factor for $SIF(t_m)$ on the right hand side of Eq. 1 is denoted daily correction factor and Fig. 1 (b) illustrates its spatial distribution and magnitude for one arbitrary orbit. In addition, the viewing-illumination geometry is important due to the directionality of the SIF emission [e.g., *Joiner et al.*, 2012; *Guanter et al.*, 2012; *Köhler et al.*, 2018; *Yang and Van Der Tol*, 2018]. Fig. 1 (c) shows the phase angle, defined as the angle between the vectors pointing from the surface pixel towards the sun and the satellite [*Hapke*, 2012]. Approaching 0° corresponds to the situation when sun and sensor are located along one axis (hot spot), with all leaves within the field of view being directly illuminated without shadowing effects. In case of low phase angles, SIF values thus are expected to be higher [on the order of 20%, *Köhler et al.*, 2018, see also Sect. S6].

The large number of TROPOMI observations (448 individual measurements per second, almost 20 times more than OCO-2) enables a unique basis for studying SIF at fine spatial and temporal scales. The exact number of valid SIF observations depends on cloud cover (see Sect. S7). We use co-located measurements from the Suomi NPP (National Polar-orbiting Partnership) VIIRS (Visible Infra-red Imaging Radiometer Suite) instrument for cloud-screening. As described in *Siddans* [2016], the S5P-NPP Cloud product contains the number of VIIRS pixels inside a TROPOMI ground pixel, which are identified as confidently cloudy, probably cloudy, probably clear, and confidently clear. In order to estimate an effective cloud cover as shown in Fig. 1 (d), we compute the weighted average of these four values using 1, 0.75, 0.25, and 0 as weights.

### 2.3. Retrieval Approach

We employed a data-driven approach similar to *Guanter et al.* [2012]; *Joiner et al.* [2013]; *Guanter et al.* [2015], and *Köhler et al.* [2015b] to separate the weak SIF emission from the reflected solar radiation. The basic measurement principle relies on the presence of solar absorption features in the solar irradiance (Fraunhofer lines). In the absence of an additive radiance source such as fluorescence, the optical depth of these absorption features remains identical even in the presence of elastic scattering by clouds, aerosols and the Earth's surface. SIF, however, changes the optical depth of Fraunhofer lines and can be computed by exploiting the change in their fractional depth with respect to non-fluorescent targets. This is realized by deriving spectral basis functions from TROPOMI data over vegetation free areas (e.g. ocean, ice, and deserts) through a singular value decomposition (SVD). A linear combination of a few spectral basis functions in combination with a reference SIF shape is then used to model spectra with a sufficient accuracy, including diverse sensor specific features. We chose a retrieval window ranging from 743 nm – 758 nm, a subset of TROPOMI's band 6. It is important to note that this wavelength range is devoid of atmospheric absorption features (water/oxygen absorption takes place in shorter/longer

wavelengths) and covers several strong solar Fraunhofer lines. Therefore, the SIF emission can pass the atmosphere without being significantly attenuated (under cloud free conditions), while maximizing the number of observed solar Fraunhofer lines reduces the sensitivity to instrumental noise. Details about the retrieval algorithm and a further assessment of the uncertainty, accuracy, and performance can be found in the supplementary information.

### 2.4. Quality Control and Filtering

Inspection and filtering of retrieval results is necessary to identify low quality SIF estimates (e.g., outliers) and potential instrumental issues such as detector nonlinearities and straylight, which could act as an additive offset that might be confused with SIF. In this context it should be noted that TROPOMI's NIR band is affected by out-of-band spectral straylight [*Kleipool et al.*, 2018]. Our initial analysis, however, shows no clear impact of straylight, i.e. there is no indication of an offset in vegetation free areas.

In order to reduce any potential impact from detector nonlinearities, we restrict the radiance level (averaged TOA radiance within the fitting window) to 20–200 $mW/m^2/sr/nm$, excluding very dark/bright scenes from our analysis. The upper radiance limit is also expected to exclude scenes with optically thick clouds, which have a shielding effect on SIF. In contrast, optical thin clouds and high aerosol loadings act as a diffuser without significantly attenuating the SIF emission [*Frankenberg et al.*, 2011a]. Here, we try to maintain as many meaningful measurements as possible by filtering only pixels with VIIRS cloud fractions larger than 0.8.

Even though the observation angle has in principle no impact on the retrieval, we evaluate only measurements with VZAs lower than 60° (corresponding to spatial rows 26–422 out of 448), because the detector pixel co-adding is reduced at the edges of the swath (see Sect. S1), leading to higher uncertainties.

Finally, potential outliers are filtered by evaluating only measurements with a $\chi_r^2$ (reduced $\chi^2$ - goodness of fit) value between 0.8 and 1.5.

A more stringent filtering ultimately depends on the desired application and requirements, e.g., only cloud free measurements, certain times of measurements, and observation geometries. Further, it is worth noting that we did not find evidence of a critically increased retrieval noise related to the South Atlantic Anomaly, which has a significant impact on GOME-2 and OCO-2 SIF retrievals, reducing data quality over parts of South America [e.g., *Köhler et al.*, 2015b; *Sun et al.*, 2018].

## 3. Results

### 3.1. Spatial Composites

We processed TROPOMI data intermittently collected from 11/23/2017 onwards. During the commissioning phase of S5-P (operational since July 2018), about half of the TROPOMI orbits were reserved for calibration activities. In Fig. 2, we present the first TROPOMI SIF maps with an unprecedented spatial resolution (global: 0.2° × 0.2°, zoom-ins: 0.05° × 0.05°). The world-map was generated by using only the center latitudes/longitudes, while the spatial

extent of each TROPOMI footprint is relevant for the zoom-ins, i.e. a SIF value contributes to a grid cell average if the footprint covers the center of this grid cell.

The maps are based on just one week of data collected during April (04/08/2018-04/15/2018) and reveal the transition from dormancy to spring in the northern hemisphere. In particular, the area south of Beijing, China, where the land use is dominated by agriculture, shows a pronounced SIF enhancement compared to other areas at similar latitudes. Consistent with our expectations, relatively high SIF values can also be observed in tropical regions, whereas barren landscapes and areas with sparse vegetation show SIF averages near zero. The Baja California zoom-in indicates that there are increased SIF values north-west of Los Angeles, especially in the San Joaquin Valley. Interestingly, a small rectangular area with relative high SIF averages can be identified south-east of Los Angeles in proximity to the Mexican border, which can be attributed to irrigated agriculture south of the Salton Sea. The zoom-in on the Nile delta indicates fairly low SIF averages during this time of year, but a pattern created by vegetation along the Nile river (typically about 15km wide) can clearly be identified. The same region is shown for a different time period (11/23/2017-11/29/2017) with overlapping data from GOME2 [*Köhler et al.*, 2015b] and OCO-2, together with the associated single-measurement precision errors.

Before applying the daily correction (Eq. 1), we scaled OCO-2 SIF (estimated at 757 nm and 771 nm) to 740 nm by $1.56 \cdot (SIF_{757nm} + 1.8 \cdot SIF_{771nm})/2$. The scaling factors were determined based on a reference SIF emission shape derived from leaf-level measurements conducted by *Magney et al.* [2017]. Fig. 3 illustrates the enormous advantage in spatial coverage of TROPOMI compared to OCO-2, despite a better spatial resolution of single OCO-2 ground pixels (2 km × 1.3 km). In contrast, GOME-2 provides a continues spatial coverage, but the coarse ground pixels (40 km × 40 km) are clearly visible, which demonstrates the potential of TROPOMI SIF to reveal detailed spatial patterns. The mean single-measurement precision errors are very similar, but the number of measurements in relation to the covered land grid cells in the Nile scene results in 15 times lower standard errors of OCO-2 compared to TROPOMI, which are in turn 8 times lower than for GOME-2.

### 3.2. Comparison between TROPOMI and OCO-2 SIF

Different satellite data sets provide a valuable tool for consistency checks, even though a global validation of space borne SIF observations with a ground truth still remains to be done. Here, we compare OCO-2 SIF (again scaled to 740 nm) and TROPOMI SIF estimates, because both satellites share the same overpass time (13:30 LST) and provide a sound basis for a comparison due to a high data rate. OCO-2 SIF can be considered the benchmark in this comparison due to a much higher spectral resolution, small ground-pixels, and a lower standard error of across-swath SIF averages. If we can tie TROPOMI to OCO-2 SIF data in regions with spatial overlap, we can use TROPOMI to virtually fill the large gaps left by OCO-2.

For the comparison in Fig. 4, we co-located the (instantaneous) SIF data acquired over land in June 2018 and evaluate only those measurements where at least ten OCO-2 measurements fall within one TROPOMI footprint. This strategy enhances the precision of OCO-2 SIF estimates, because the standard error of the mean is at least three times ($\sqrt{10}$) lower

compared to the uncertainty of a single measurement. The TROPOMI SIF filtering was very strict so that the OCO-2 observations are closely matched. Specifically, the difference in time of measurement/observational phase angle was limited to 10 min./20° and the maximum cloud fraction of the TROPOMI measurements was set to 0.1. The following analysis is, therefore, based on only 1,125 TROPOMI and 14,917 OCO-2 measurements.

The spread between (single) TROPOMI SIF estimates and (averaged) OCO-2 SIF is highly consistent with our expectations, because the standard deviation of the differences (0.44 $mW/m^2/sr/nm$) is in agreement with the TROPOMI single-measurement precision error (~ 0.4 $mW/m^2/sr/nm$, see Sect. S4&S5). The retrieval noise explains negative SIF values, which occur primarily for single TROPOMI measurements, illustrating that single measurements should not be over-interpreted. In a next step, either 2, 5, or 10 TROPOMI measurements were aggregated latitudinally, resulting in a convergence of both data sets in terms of correlation and absolute SIF values. It is noteworthy that the different aggregation levels lead to a predictable decrease in the spread. We find a remarkable correspondence with a regression slope close to one and a $R^2$ value of 0.88 when ten TROPOMI measurements are aggregated. In this case, the standard deviation of the differences between TROPOMI and OCO-2 SIF decreases to 0.18 $mW/m^2/sr/nm$, close to the theoretically expected value of 0.14 $mW/m^2/sr/nm$. A further assessment of the latitudinal consistency between OCO-2 and TROPOMI SIF can be found in Sect. S8.

## 4. Conclusion

We presented the first TROPOMI SIF retrievals along with essential instrument specific measurement features and an initial comparison to the independent OCO-2 SIF data set. In general, our results meet the high expectations of TROPOMI SIF measurements, which were anticipated by *Guanter et al.* [2015]. We observe no indication of potential instrumental artifacts such as straylight in the retrieval. The combination of TROPOMI's spectral resolution, radiometric accuracy/SNR, wide swath (allowing for almost daily surface coverage), and ground pixel size of about 7 km × 3.5 km (at nadir) largely outperforms previous and existing capabilities for a spatial continuous monitoring of SIF. The excellent radiometric performance also allows us to use a much narrower fitting window, which is devoid of atmospheric absorption features and thus minimizes interferences with atmospheric trace gas absorptions. In particular, the spatio-temporal resolution of global SIF averages has the promising potential to leverage future investigations aiming to evaluate the SIF-GPP relationship at ecologically meaningful scales. The inter-sensor comparison between TROPOMI and OCO-2 SIF data shows a very strong agreement, suggesting that the TROPOMI SIF data are of comparable quality for individual measurements but with largely improved spatial and temporal coverage.

## Supplementary Material

Refer to Web version on PubMed Central for supplementary material.

## Acknowledgments.

This work was funded by the EARTH SCIENCE U.S. PARTICIPATING INVESTIGATOR (Grant Number: NNX15AH95G). Sentinel-5 Precursor is a European Space Agency (ESA) mission implemented on behalf of the European Commission (EC). The TROPOMI payload is a joint development by ESA and the Netherlands Space Office (NSO). The Sentinel-5 Precursor ground segment development has been funded by ESA and with national contributions from The Netherlands, Germany, Belgium and UK. The OCO-2 SIF data was produced by the OCO-2 project at the Jet Propulsion Laboratory, California Institute of Technology, and obtained from the OCO-2 data archive maintained at the NASA Goddard Earth Science Data and Information Services Center. The TROPOMI SIF data can be accessed through ftp://fluo.gps.caltech.edu/data/tropomi/.

## References

Borsdorff T, Aan de Brugh J, Hu H, Aben I, Hasekamp O, and Landgraf J. (2018), Measuring carbon monoxide with TROPOMI: First results and a comparison with ECMWF-IFS analysis data, Geophysical Research Letters, 45(6), 2826–2832.

Crisp D, Pollock HR, Rosenberg R, Chapsky L, Lee RA, Oyafuso FA, Frankenberg C, O'Dell CW, Bruegge CJ, Doran GB, et al. (2017), The on-orbit performance of the orbiting carbon observatory-2 (oco-2) instrument and its radiometrically calibrated products, Atmospheric Measurement Techniques, 10(1), 59.

Frankenberg C, Butz A, and Toon G. (2011a), Disentangling chlorophyll fluorescence from atmospheric scattering effects in o2 a-band spectra of reflected sun-light, Geophysical Research Letters, 38(3).

Frankenberg C, Fisher JB, Worden J, Badgley G, Saatchi SS, Lee J-E, Toon GC, Butz A, Jung M, Kuze A, et al. (2011b), New global observations of the terrestrial carbon cycle from gosat: Patterns of plant fluorescence with gross primary productivity, Geophysical Research Letters, 38(17).

Guan K, Pan M, Li H, Wolf A, Wu J, Medvigy D, Caylor KK, Sheffield J, Wood EF, Malhi Y, et al. (2015), Photosynthetic seasonality of global tropical forests constrained by hydroclimate, Nature Geoscience, 8(4), 284–289.

Guanter L, Frankenberg C, Dudhia A, Lewis PE, Gómez-Dans J, Kuze A, Suto H, and Grainger RG (2012), Retrieval and global assessment of terrestrial chlorophyll fluorescence from GOSAT space measurements, Remote Sensing of Environment, 121, 236–251.

Guanter L, Rossini M, Colombo R, Meroni M, Frankenberg C, Lee J-E, and Joiner J. (2013), Using field spectroscopy to assess the potential of statistical approaches for the retrieval of sun-induced chlorophyll fluorescence from ground and space, Remote Sensing of Environment, 133, 52–61.

Guanter L, Zhang Y, Jung M, Joiner J, Voigt M, Berry JA, Frankenberg C, Huete AR, Zarco-Tejada P, Lee J-E, et al. (2014), Global and time-resolved monitoring of crop photosynthesis with chlorophyll fluorescence, Proceedings of the National Academy of Sciences, 111(14), E1327–E1333.

Guanter L, Aben I, Tol P, Krijger J, Hollstein A, Köhler P, Damm A, Joiner J, Frankenberg C, and Landgraf J. (2015), Potential of the tropospheric monitoring instrument (tropomi) onboard the sentinel-5 precursor for the monitoring of terrestrial chlorophyll fluorescence, Atmospheric Measurement Techniques, 8(3), 1337–1352.

Hapke B. (2012), Theory of reflectance and emittance spectroscopy, Cambridge University Press.

Hu H, Landgraf J, Detmers R, Borsdorff T, de Brugh JA, Aben I, Butz A, and Hasekamp O (), Toward global mapping of methane with tropomi: First results and intersatellite comparison to gosat, Geophysical Research Letters, 0(0), doi: 10.1002/2018GL077259.

Jeong S-J, Schimel D, Frankenberg C, Drewry DT, Fisher JB, Verma M, Berry JA, Lee J-E, and Joiner J. (2017), Application of satellite solar-induced chlorophyll fluorescence to understanding large-scale variations in vegetation phenology and function over northern high latitude forests, Remote sensing of environment, 190, 178–187.

Joiner J, Yoshida Y, Vasilkov A, Middleton E, and Corp L. (2011), First observations of global and seasonal terrestrial chlorophyll fluorescence from space, Biogeosciences, 8(3), 637–651.

Joiner J, Yoshida Y, Vasilkov A, Middleton E, Campbell P, Kuze A, and Corp L. (2012), Filling-in of near-infrared solar lines by terrestrial fluorescence and other geophysical effects: Simulations and

space-based observations from SCIAMACHY and GOSAT, Atmospheric Measurement Techniques, 5(4), 809–829.

Joiner J, Guanter L, Lindstrot R, Voigt M, Vasilkov A, Middleton E, Huemmrich K, Yoshida Y, and Frankenberg C. (2013), Global monitoring of terrestrial chlorophyll fluorescence from moderate-spectral-resolution near-infrared satellite measurements: methodology, simulations, and application to GOME-2, Atmospheric Measurement Techniques, 6(10), 2803–2823.

Kleipool Q, Ludewig A, Babic L, Bartstra R, Braak R, Dierssen W, Dewitte P-J, Kenter P, Landzaat R, Leloux J, Loots E, Meijering P, van der Plas E, Rozemeijer N, Schepers D, Schiavini D, Smeets J, Vacanti G, Vonk F, and Veefkind P. (2018), Pre-launch calibration results of the tropomi payload on-board the sentinel 5 precursor satellite, Atmospheric Measurement Techniques Discussions, 2018, 1–67, doi: 10.5194/amt-2018-25.

Köhler P, Guanter L, and Frankenberg C. (2015a), Simplified Physically Based Retrieval of Sun-Induced Chlorophyll Fluorescence From GOSAT Data, Geoscience and Remote Sensing Letters, IEEE, 12(7), 1446–1450.

Köhler P, Guanter L, and Joiner J. (2015b), A linear method for the retrieval of sun-induced chlorophyll fluorescence from GOME-2 and SCIAMACHY data, Atmospheric Measurement Techniques, 8(6), 2589–2608.

Köhler P, Guanter L, Kobayashi H, Walther S, and Yang W. (2018), Assessing the potential of sun-induced fluorescence and the canopy scattering coefficient to track large-scale vegetation dynamics in amazon forests, Remote Sensing of Environment, 204, 769–785.

Lee J-E, Frankenberg C, van der Tol C, Berry JA, Guanter L, Boyce CK, Fisher JB, Morrow E, Worden JR, Asefi S, Badgley G, and Saatchi S. (2013), Forest productivity and water stress in Amazonia: observations from GOSAT chlorophyll fluorescence, Proceedings of the Royal Society of London B: Biological Sciences, 280(1761).

MacBean N, Maignan F, Bacour C, Lewis P, Peylin P, Guanter L, Köhler P, Gómez-Dans J, and Disney M. (2018), Strong constraint on modelled global carbon uptake using solar-induced chlorophyll fluorescence data, Scientific reports, 8(1), 1973. [PubMed: 29386626]

Magney TS, Frankenberg C, Fisher JB, Sun Y, North GB, Davis TS, Kornfeld A, and Siebke K. (2017), Connecting active to passive fluorescence with photosynthesis: a method for evaluating remote sensing measurements of Chl fluorescence, New Phytologist, 215(4), 1594–1608. [PubMed: 28664542]

Parazoo NC, Bowman K, Frankenberg C, Lee J-E, Fisher JB, Worden J, Jones D, Berry J, Collatz GJ, Baker IT, et al. (2013), Interpreting seasonal changes in the carbon balance of southern Amazonia using measurements of $XCO_2$ and chlorophyll fluorescence from GOSAT, Geophysical Research Letters, 40(11), 2829–2833.

Parazoo NC, Bowman K, Fisher JB, Frankenberg C, Jones D, Cescatti A, Pérez- Priego Ó, Wohlfahrt G, and Montagnani L. (2014), Terrestrial gross primary production inferred from satellite fluorescence and vegetation models, Global change biology, 20(10), 3103–3121. [PubMed: 24909755]

Porcar-Castell A, Tyystjärvi E, Atherton J, van der Tol C, Flexas J, Pfündel EE, Moreno J, Frankenberg C, and Berry JA (2014), Linking chlorophyll a fluorescence to photosynthesis for remote sensing applications: mechanisms and challenges, Journal of Experimental Botany.

Siddans R. (2016), S5P-NPP Cloud Processor ATBD, Report.

Sun K, Liu X, Nowlan CR, Cai Z, Chance K, Frankenberg C, Lee RA, Pollock R, Rosenberg R, and Crisp D. (2017), Characterization of the oco-2 instrument line shape functions using on-orbit solar measurements, Atmospheric Measurement Techniques, 10(3), 939.

Sun Y, Frankenberg C, Jung M, Joiner J, Guanter L, Köhler P, and Magney T. (2018), Overview of solar-induced chlorophyll fluorescence (sif) from the orbiting carbon observatory-2: Retrieval, cross-mission comparison, and global monitoring for gpp, Remote Sensing of Environment, 209, 808–823.

Thum T, Zaehle S, Köhler P, Aalto T, Aurela M, Guanter L, Kolari P, Laurila T, Lohila A, Magnani F, et al. (2017), Modelling sun-induced fluorescence and photosynthesis with a land surface model at local and regional scales in northern europe, Biogeosciences, 14(7), 1969.

Veefkind J, Aben I, McMullan K, Förster H, De Vries J, Otter G, Claas J, Eskes H, De Haan J, Kleipool Q, et al. (2012), Tropomi on the esa sentinel-5 precursor: A gmes mission for global observations of the atmospheric composition for climate, air quality and ozone layer applications, Remote Sensing of Environment, 120, 70–83.

Verma M, Schimel D, Evans B, Frankenberg C, Beringer J, Drewry DT, Magney T, Marang I, Hutley L, Moore C, et al. (2017), Effect of environmental conditions on the relationship between solar-induced fluorescence and gross primary productivity at an ozflux grassland site, Journal of Geophysical Research: Biogeosciences, 122(3), 716–733.

Walther S, Voigt M, Thum T, Gonsamo A, Zhang Y, Köhler P, Jung M, Varlagin A, and Guanter L. (2016), Satellite chlorophyll fluorescence measurements reveal large-scale decoupling of photosynthesis and greenness dynamics in boreal evergreen forests, Global change biology, 22(9), 2979–2996. [PubMed: 26683113]

Wolanin A, Rozanov V, Dinter T, Nöel S, Vountas M, Burrows J, and Bracher A. (2015), Global retrieval of marine and terrestrial chlorophyll fluorescence at its red peak using hyperspectral top of atmosphere radiance measurements: Feasibility study and first results, Remote Sensing of Environment, 166, 243–261.

Wood JD, Griffis TJ, Baker JM, Frankenberg C, Verma M, and Yuen K. (2017), Multiscale analyses of solar-induced florescence and gross primary production, Geophysical Research Letters, 44(1), 533–541.

Yang P, and Van Der Tol C. (2018), Linking canopy scattering of far-red sun-induced chlorophyll fluorescence with reflectance, Remote Sensing of Environment, 209, 456–467.

Yang X, Tang J, Mustard JF, Lee J-E, Rossini M, Joiner J, Munger JW, Kornfeld A, and Richardson AD (2015), Solar-induced chlorophyll fluorescence that correlates with canopy photosynthesis on diurnal and seasonal scales in a temperate deciduous forest, Geophysical Research Letters, 42(8), 2977–2987.

Zhang Y, Guanter L, Berry JA, Joiner J, Tol C, Huete A, Gitelson A, Voigt M, and Köhler P. (2014), Estimation of vegetation photosynthetic capacity from space-based measurements of chlorophyll fluorescence for terrestrial biosphere models, Global change biology, 20(12), 3727–3742. [PubMed: 24953485]

Zhang Y, Xiao X, Jin C, Dong J, Zhou S, Wagle P, Joiner J, Guanter L, Zhang Y, Zhang G, et al. (2016), Consistency between sun-induced chlorophyll fluorescence and gross primary production of vegetation in north america, Remote Sensing of Environment, 183, 154–169.

**Keypoints:**

- First solar induced chlorophyll fluorescence (SIF) observations from TROPOMI near-infrared band measurements
- Unprecedented spatio-temporal resolution of global SIF maps
- Inter-sensor comparison between TROPOMI and OCO-2 SIF data shows excellent agreement

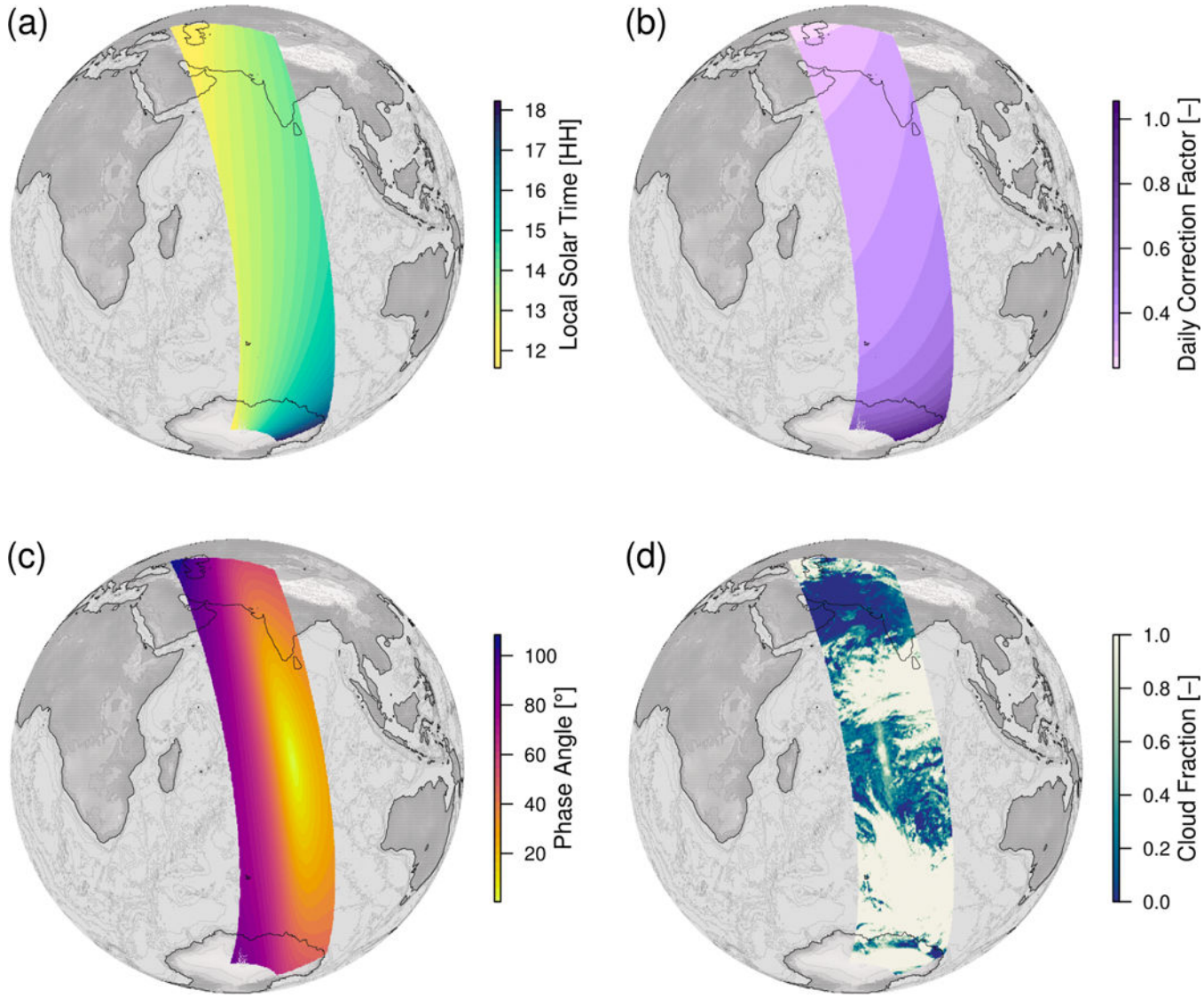


**Figure 1.**

An arbitrary orbit (solar zenith angles lower than 70°) is shown to illustrate (a) local solar times, (b) daily correction factors from Eq.1, (c) observational phase angles, and (d) cloud fraction derived from co-located VIIRS-NPP data.

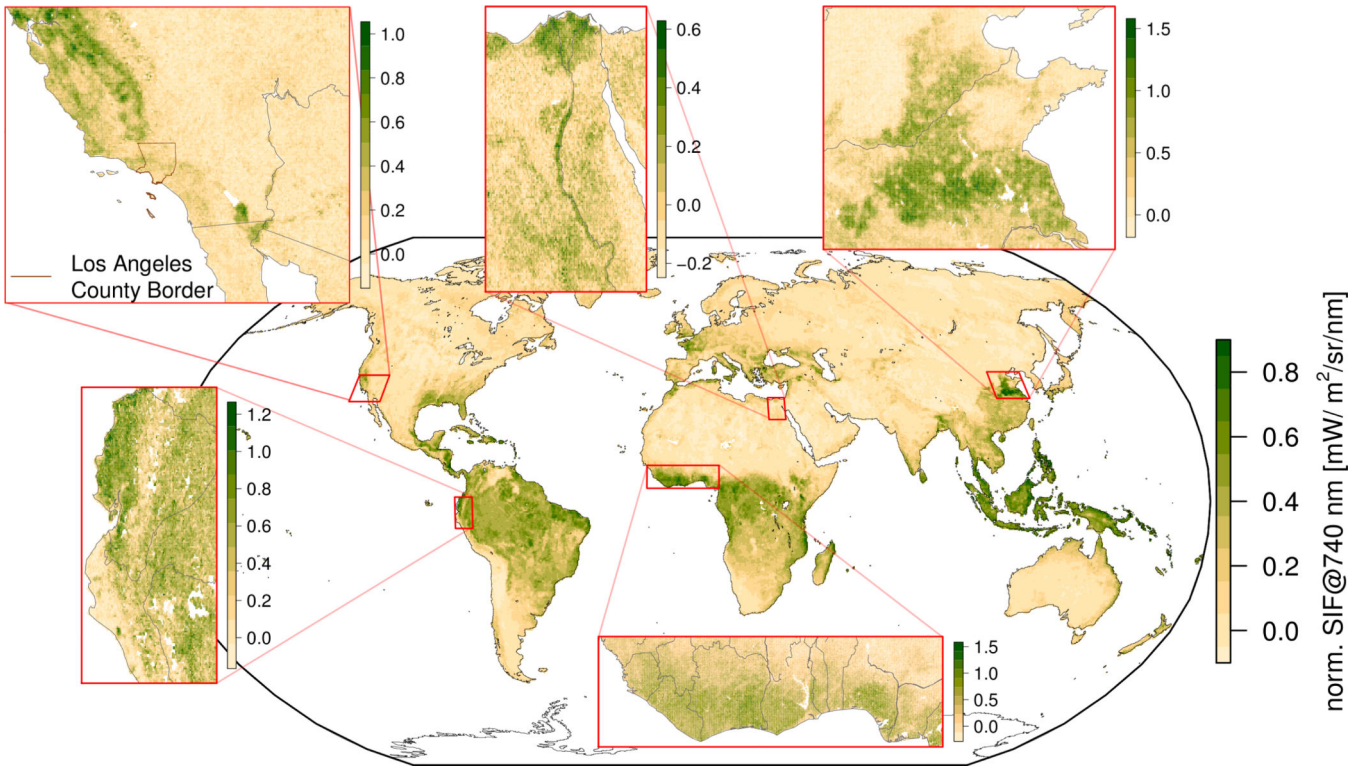


**Figure 2.**

The global SIF map is based on data acquired between 04/08/2018 and 04/15/2018 (114 orbits, 16M measurements over land). Retrieval results were normalized (Eq. 1) and gridded to a spatial resolution of 0.2° × 0.2°. The zoom-ins are gridded to 0.05° × 0.05°.

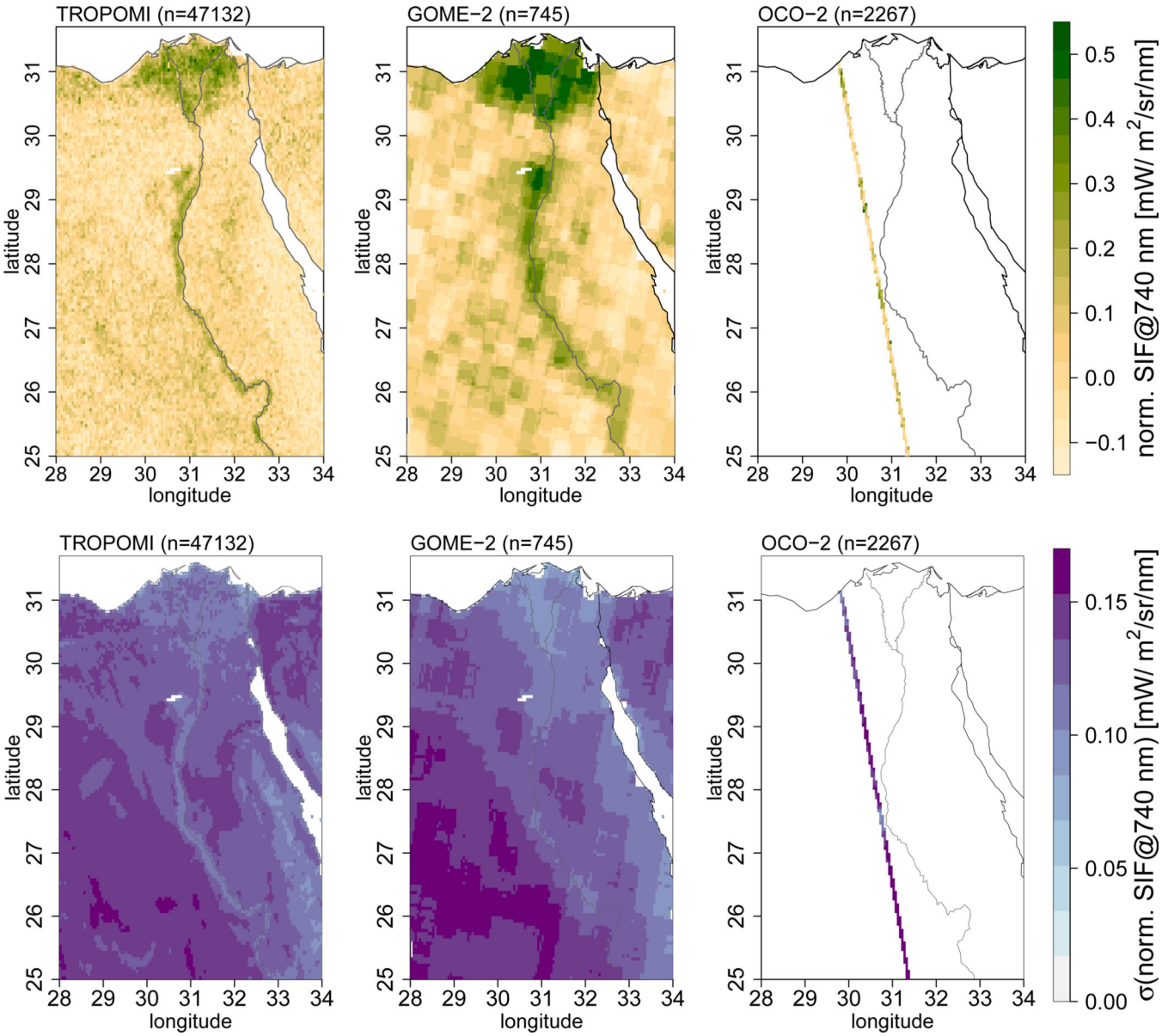


**Figure 3.**

Comparison between TROPOMI, GOME-2, and OCO-2 SIF together with the associated mean single-measurement precision errors in the Nile region based on data acquired between 11/23/2017 and 11/29/2017 (n denotes the number of included soundings). Retrieval results were normalized (Eq. 1) and gridded to a spatial resolution of 0.05° × 0.05°.

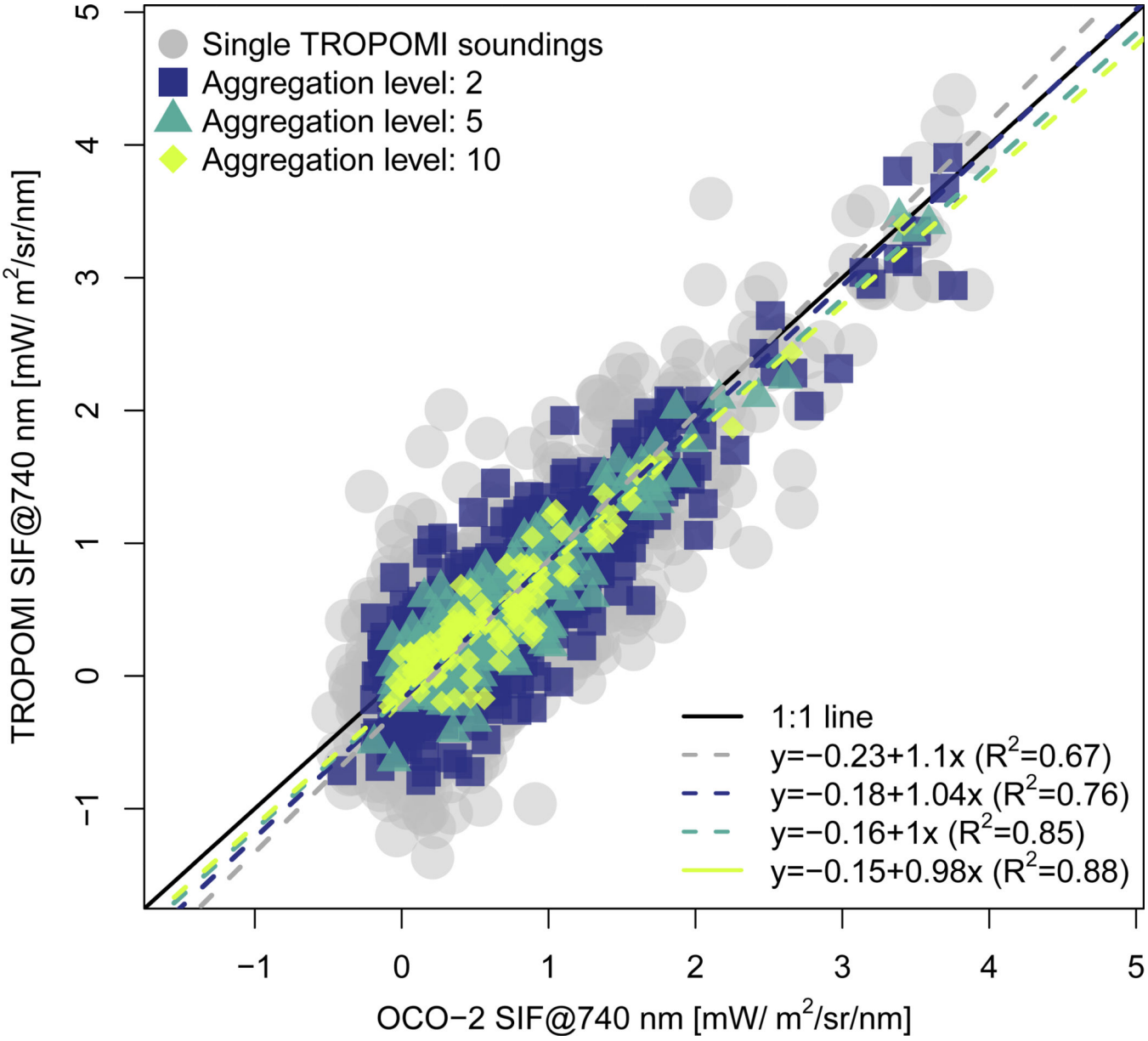


**Figure 4.**
Comparison between TROPOMI and OCO-2 SIF, based on data collected in June 2018. Note that at least ten OCO-2 measurements fall within one TROPOMI footprint. Color codes indicate that either 2, 5, or 10 TROPOMI measurements were aggregated latitudinally.